Reduction of NF can be achieved by further optimizing the DP structure, like adding a segment of forward pumped EDF [15], or incorporating a fiber Bragg grating [16].

3. CONCLUSION

We have demonstrated a high power EDFA for signal amplification in the wavelength range from 1570 to 1620 nm. The output saturated power can be greatly enhanced by employing clad-pumping technology in a DP configuration. The characteristics of optical PCE, signal gain, and NF are well discussed, both for single- and DP structures. The DP system has achieved a high output power over 2 W and a flat-gain about 23 dB, which is ~3 dB higher than that of the SP system. Experimental results also show dramatic increase in PCE and some degree of NF deterioration.

ACKNOWLEDGMENT

This work was supported by Zhejiang Provincial Natural Science Foundation of China (Grant No. LQ13F050009), and Zhejiang Province science and technology plan projects (Grant No. 2014C31066 and 2013C31094).

REFERENCES

1. B. Perez-Hettera, A. Ullan, D. Leandro, M. Fernandez-Vallejo, M. Quintela, A. Loayssa, J. Lopez-Higuera, and M. Lopez-Amo, L-band multiwavelength single-longitudinal mode fiber laser for sensing applications, J Lightwave Technol 30 (2012), 1173–1177.
2. A. Bellemare, M. Karasek, C. Riviere, F. Babin, G. He, V. Roy, and G. Schim, A broadly tunable erbium-doped fiber ring laser: Experimentation and modeling, IEEE J Sel Top Quantum Electron 7 (2001), 22–29.
3. B. Min, H. Yoon, W. Leee, and N. Park, Coupled structure for wide-band EDFA with gain and noise figure improvements from C to L-band ASE injection, IEEE Photonics Technol Lett 12 (2000), 480–482.
4. M. Jinno, T. Sakamoto, J. Kani, S. Aisawa, K. Oda, M. Fukui, H. Ono, and K. Oguchi, First demonstration of 1580 nm wavelength band WDM transmission for doubling usable bandwidth and suppressing FWM in DSF, Electron Lett 33 (1997), 882–883.
5. X. Cheng, R. Parvizi, H. Ahmad, and S. Harun, Wide-band bismuth-based erbium-doped fiber amplifier with a flat-gain characteristic, IEEE Photonics J 1 (2009), 259–264.
6. A. Mori, T. Sakamoto, K. Kobayashi, K. Shikano, K. Oikawa, K. Hoshino, T. Kanamori, Y. Ohishi, and M. Shimizu, 1.58 um broadband erbium doped tellurite fiber amplifier, J Lightwave Technol 20 (2002), 822–827.
7. S. Singh and R. Kaler, Flat-gain L-band Raman-EDFA hybrid optical amplifier for dense wavelength division multiplexed system, IEEE Photonics Technol Lett 25 (2013), 250–252.
8. J. Lee, U. Ryn, S. Ahn, and N. Park, Enhancement of power conversion efficiency for an L-band EDFA with a secondary pumping effect in the unpumped EDF section, IEEE Photonics Technol Lett 11 (1999), 42–44.
9. H. Chung, M. Lee, D. Lee, N. Park, and D. DiGiovanni, Low noise, high efficiency L-band EDFA with 980nm pumping, Electron Lett 35 (1999), 1099–1100.
10. C. Yeh, C. Chen, C. Lee, and S. Chi, Wide-band two-stage erbium-doped fiber amplifier module in parallel configuration, Jpn J Appl Phys 44 (2005), 239–240.
11. N. Yusoff, A. Abas, S. Hitam, and M. Mahdi, Dual-stage L-band erbium-doped fiber amplifier with distributed pumping from single pump laser, Opt Commun 285 (2012), 1383–1386.
12. S. Harun, P. Poopalan, and H. Ahmad, Gain enhancement in L-band EDFA through a double-pass technique, IEEE Photonics Technol Lett 14 (2002), 296–297.
13. T. Liang, N. Cheng, and S. Hung, Gain enhancement in L-band gain-flattened EDFA using a reflective-type structure, Microwave Opt Technol Lett 37 (2003), 393–395.
14. S. Harun, N. Tamchek, P. Poopalan, and H. Ahmad, Gain improvement in L-band EDFA using unpumped EDF in a double pass system, Microwave Opt Tech Lett 36 (2003), 154–156.
15. S. Harun, N. Tamchek, P. Poopalan, and H. Ahmad, Double-pass L-band EDFA with enhanced noise figure characteristics, IEEE Photonics Technol Lett 15 (2003), 1055–1057.
16. L. Yi, L. Zhan, J. Ji, Q. Ye, and Y. Xia, Improvement of gain and noise figure in double-pass L-band EDFA by incorporating a fiber Bragg grating, IEEE Photonics Technol Lett 16 (2004), 1005–1007.
17. C. Chang, L. Wang, and Y. Chiang, A dual pumped double-pass L-band EDFA with high gain and low noise, Opt Commun 267 (2006), 108–112.
18. B. Zhu, M. Law, J. Rooney, S. Shenk, M. Yan, and D. DiGiovanni, High-power broadband Yb-free clad-pumped EDFA for L-band DWDM applications, Opt Lett 39 (2014), 72–75.

DUAL-INVERTED-F ANTENNA WITH A DECOUPLING CHIP INDUCTOR FOR THE 3.6-GHZ LTE OPERATION IN THE TABLET COMPUTER

Kin-Lu Wong and Li-Yu Chen
Department of Electrical Engineering, National Sun Yat-Sen University, Gushan, Kaohsiung 80424, Taiwan; Corresponding author: wongkl@ema.ee.nsysu.edu.tw

Received 2 March 2015

ABSTRACT: *A simple, decoupled dual-inverted-F antenna (DIFA) formed by two inverted-F antennas (IFAs) with a decoupling chip inductor is presented. The open ends of the two IFAs face to each other and are connected by the decoupling chip inductor. The DIFA has a planar structure and is easily fabricated on a thin dielectric substrate. Good isolation between the two IFAs can be obtained, owing to an equivalent bandstop circuit formed by the decoupling chip inductor and the equivalent distributed capacitor between the open ends of the two IFAs. For the tablet computer application in the 3.6-GHz LTE band (3.4–3.8 GHz), the DIFA with a decoupling chip inductor of 39 nH occupies a small size of 20 × 4 mm^2 on a 0.8-mm thick FR4 substrate. The two IFAs in the DIFA almost require no isolation spacing, thereby leading to the compact structure and small size. Details of the proposed DIFA are described, and its multi-input multioutput performance is discussed.* © 2015 Wiley Periodicals, Inc. Microwave Opt Technol Lett 57:2189–2194, 2015; View this article online at wileyonlinelibrary.com. DOI 10.1002/mop.29288

Key words: *mobile antennas; inverted-F antennas; dual-inverted-F antenna; LTE antennas; decoupling inductor; tablet computer antennas*

1. INTRODUCTION

For the MIMO (Multi-input Multioutput) operation in the terminal device, two or more antennas with acceptable isolation are required to be embedded in the limited space therein. However, when two antennas are placed very close to each other, strong coupling thereof usually occurs, which greatly decreases the antenna efficiency and MIMO performance as well. To decrease the coupling between two closely spaced antennas, it has been shown that the technique of using a single neutralization line (NL) or multiple NLs can be applied [1–6]. By selecting proper length and width of the NL and their proper connections with the two closely spaced antennas, improved isolation can be obtained. However, the design process in determining the

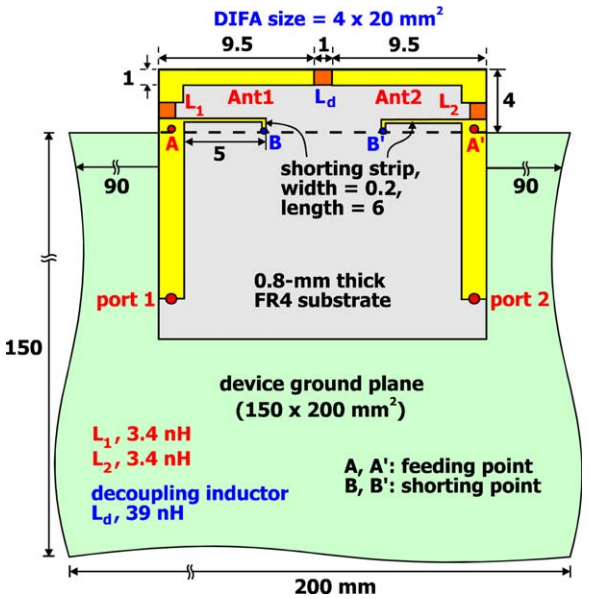

Figure 1 Geometry of the DIFA mounted at the center of the top (long) edge of the device ground plane of the tablet computer. [Color figure can be viewed in the online issue, which is available at wileyonlinelibrary.com]

parameters of the NL is usually time consuming. Moreover, as the required length of the NL is generally comparable to a quarter-wavelength at the desired operating frequency, a certain space to accommodate the NL between the two antennas is required. This increases the complexity of the antenna design for the MIMO operation.

In this article, we propose a simple dual-inverted-F antenna (DIFA) with acceptable isolation obtained for the 3.6-GHz LTE operation (3.4–3.8 GHz) [7,8] in the tablet computer. The DIFA has a planar structure and occupies a small size of 20 × 4 mm^2 on a 0.8-mm thick FR4 substrate. The DIFA is formed by two face-to-face inverted-F antennas (IFAs) with a decoupling chip inductor of 39 nH connected between their open ends to enhance the isolation of the two IFAs. In this case, the two

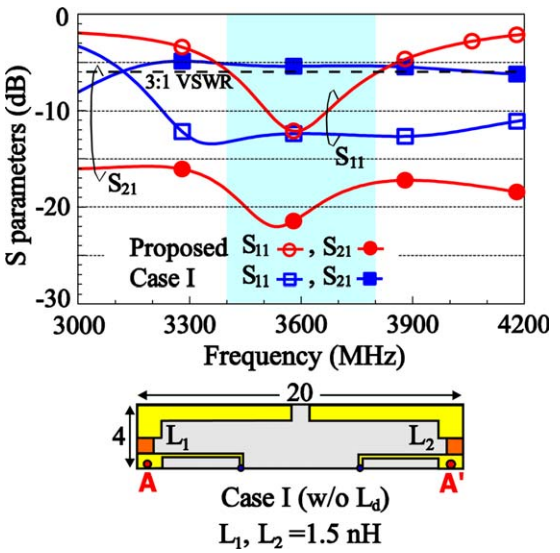

Figure 2 Simulated *S* parameters for the proposed DIFA and the case without the inductor L_d (Case I). [Color figure can be viewed in the online issue, which is available at wileyonlinelibrary.com]

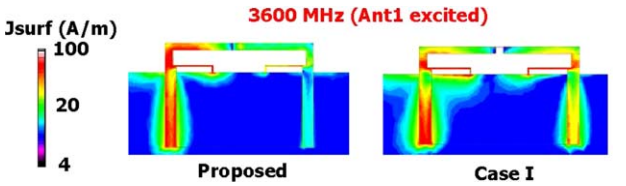

Figure 3 Simulated surface current distributions for the proposed DIFA and Case I. [Color figure can be viewed in the online issue, which is available at wileyonlinelibrary.com]

IFAs almost require no isolation spacing and can hence lead to a compact size for the DIFA. In addition, as compared to the design using the NL technique [1–6], the proposed DIFA is simple in structure and can be easily implemented. The measured isolation between the two IFAs in the proposed DIFA is better than about 16.5 dB over the 3.6-GHz band. Measured antenna efficiencies of about 50–74% for the two IFAs are also obtained. In this study, details of the proposed DIFA are described. Its working principle, parametric study, experimental results, and MIMO performance are also presented and discussed.

2. PROPOSED DIFA

2.1. Antenna Structure

Figure 1 shows the geometry of the DIFA mounted at the center of the top (long) edge of the device ground plane of the tablet computer. The DIFA is formed by two IFAs (Ant1 and Ant2) with same dimensions and a chip inductor L_d connecting the two IFAs at their open ends. Ant1 is excited by port 1, while Ant2 is excited by port 2. The dimensions of the device ground plane are selected to be 200 × 150 mm^2 to fit for the popular 9.7-inch tablet computer on the market. For operating in the 3.6-GHz band (3.4–3.8 GHz), the DIFA has a planar structure and occupies a small size of 4 × 20 mm^2 on a thin FR4 substrate of thickness 0.8 mm, relative permittivity 4.4, and loss tangent 0.02.

Each IFA is designed to have a low profile of 4 mm and a strip length of 13.5 mm only (about 0.16 wavelength at 3.6 GHz). For achieving the low profile and short strip length, each IFA is loaded with a chip inductor of 3.4 nH (L_1, L_2) and is short-circuited to the device ground plane through a shorting strip of length 6 mm and width 0.2 mm. The chip inductors of L_1 and L_2 decrease the required resonant length for the two IFAs [9]. The two IFAs are also arranged to face each other, with their open ends having a small spacing of 1 mm only.

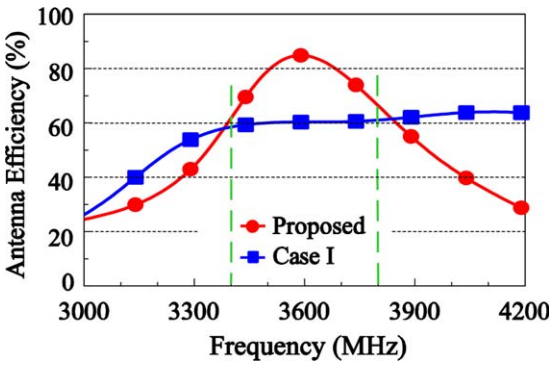

Figure 4 Simulated antenna efficiency for the proposed DIFA and Case I. [Color figure can be viewed in the online issue, which is available at wileyonlinelibrary.com]

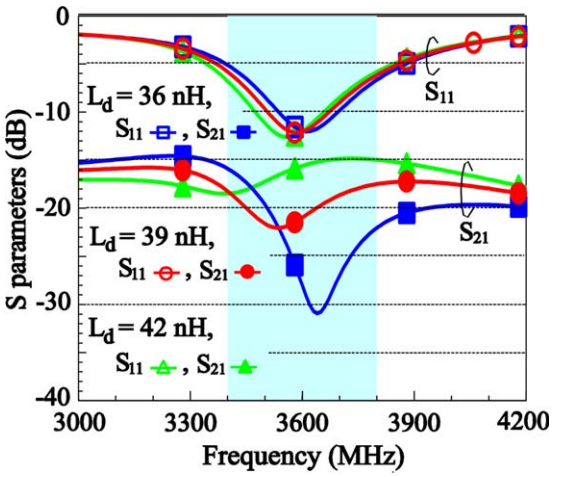

Figure 5 Simulated S parameters as a function of the chip inductor L_d for the proposed DIFA. [Color figure can be viewed in the online issue, which is available at wileyonlinelibrary.com]

Owing to the small spacing, there is strong capacitive coupling between the two IFAs. This behavior is very likely related to an equivalent distributed capacitor formed between the two open ends. By disposing a chip inductor of 39 nH (L_d) in-between and connecting the two open ends, it is found that the strong capacitive coupling can be effectively decreased. This is largely because the loaded chip inductor and the equivalent distributed capacitor between the two open ends can form a bandstop circuit to effectively decrease the coupling between the two IFAs. Hence, it is expected that by selecting the chip inductor of different inductances, the decoupling effect on the two IFAs can be adjusted. Related results will be discussed in the next subsection.

It is also noted that owing to the very small spacing between the two IFAs, the DIFA has a compact structure. With a low profile of 4 mm only, the DIFA has a short length of 20 mm (about 0.24 wavelength at 3.6 GHz) along the top edge of the device ground plane. In addition, with the proposed structure, the DIFA generally shows an inverted-U shape, with the two shorting strips enclosed therein. The DIFA also shows a closed loop structure with no open ends. That is, the possible coupling between the DIFA and nearby possible electronic elements inside the tablet computer can be small. This will be attractive for the practical applications.

2.2. Working Principle and Parametric Study

Effects of the inductor L_d are first analyzed. Figure 2 shows the simulated S parameters for the proposed DIFA and the case without the inductor L_d (Case I, see the structure in the figure). The dimensions of the two IFAs in Case I are the same as those in the proposed DIFA. The simulated results are obtained using the full-wave electromagnetic field simulator HFSS version 15 [10]. As the two IFAs (Ant1 and Ant2) are symmetric with respect to the center of the top edge of the device ground plane, the simulated S_{11} and S_{22} results are the same. Hence, only the results for the S_{11} are shown. Both the S_{11} results for the proposed DIFA and Case I are adjusted to be better than −6 dB over the 3.6-GHz band (3.4–3.8 GHz, see the shaded frequency region in the figure). Note that in Case I, because there is no decoupling chip inductor L_d, the inductors L_1 and L_2 embedded in the two IFAs are changed to be 1.5 nH so that the resonant mode of the two IFAs can occur in the 3.6-GHz band. It is observed that Case I shows much better impedance matching

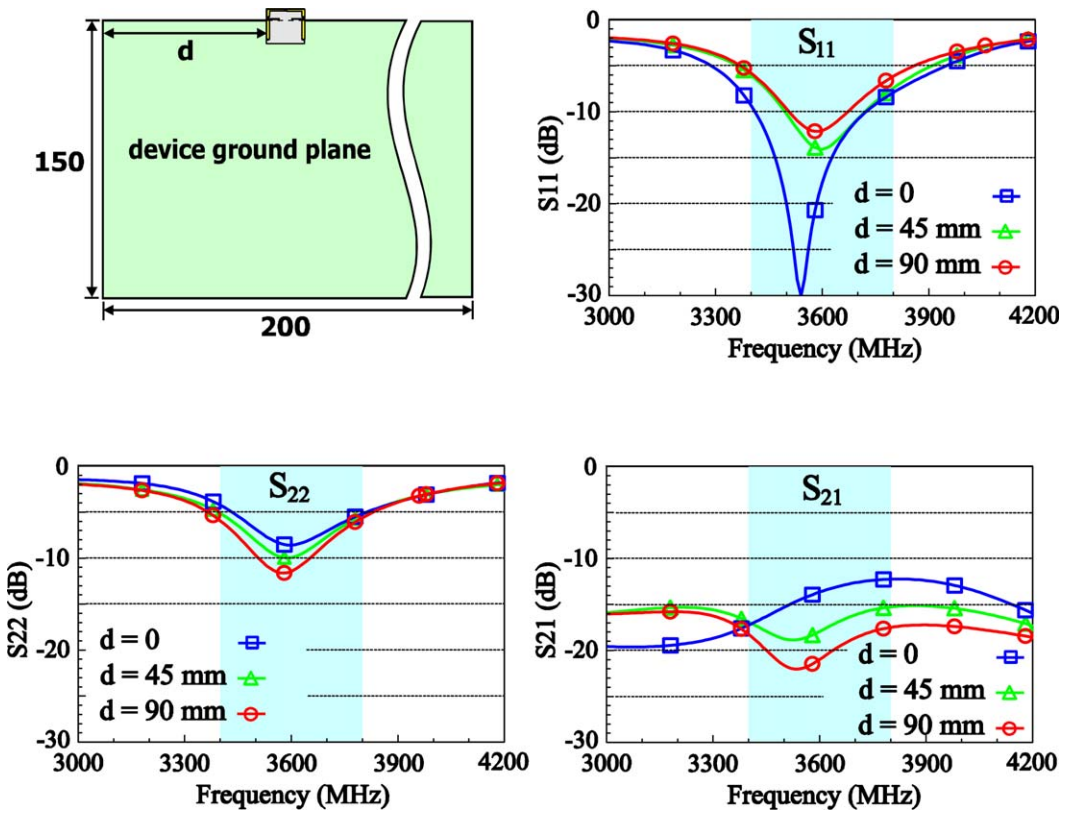

Figure 6 Simulated S parameters for the proposed DIFA mounted at different positions along the top edge of the device ground plane. [Color figure can be viewed in the online issue, which is available at wileyonlinelibrary.com]

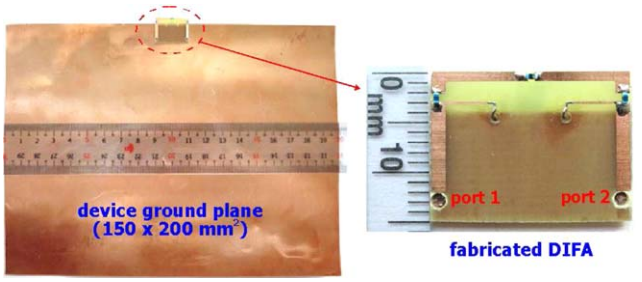

Figure 7 Photos of the fabricated DIFA. [Color figure can be viewed in the online issue, which is available at wileyonlinelibrary.com]

than the proposed DIFA. However, its S_{21} is only about −5 dB over the operating band, which is much larger than that (less than about −17.5 dB) of the proposed DIFA. The obtained results indicate that Case I has strong coupling between its two IFAs therein. This behavior is owing to the very small spacing between the open ends of the two IFAs. Conversely, much smaller S_{21} is obtained for the proposed DIFA, which is owing to the presence of the inductor L_d.

The simulated surface current distributions for the proposed DIFA and Case I at 3.6 GHz are also shown in Figure 3 for comparison. It is seen that with Ant1 excited, the excited surface current distributions on Ant2 is relatively much smaller for the proposed DIFA than for Case I. This also confirms that good decoupling between the two IFAs is obtained for the proposed DIFA. This behavior is largely because the inductor L_d and the equivalent distributed capacitor between the open ends of the two IFAs form an equivalent bandstop circuit, which suppresses the possible coupling between the two IFAs.

Figure 4 shows the simulated antenna efficiency for the proposed DIFA and Case I. The antenna efficiencies include the mismatching losses. Results show that the proposed DIFA has better efficiencies than Case I (62–84% vs. 59–61% over the operating band). At 3.6 GHz, the efficiency of the proposed DIFA is about 24% better than that of Case I.

As it is likely that the inductor L_d and the distributed capacitor between the two open ends form a bandstop circuit to achieve good decoupling between the two IFAs, the S_{21} result of the proposed DIFA can be controlled by adjusting the inductance of the inductor L_d. Figure 5 shows the simulated S parameters as a function of the chip inductor L_d. Results for the L_d varied from 36 to 42 nH are presented. Small effects on the S_{11} results are seen. Conversely, large effects on the S_{21} are

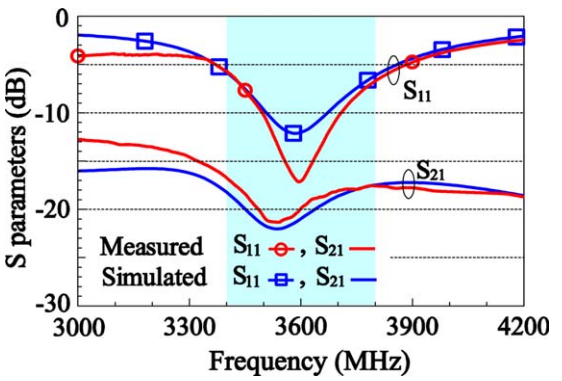

Figure 8 Measured and simulated S parameters of the fabricated DIFA. [Color figure can be viewed in the online issue, which is available at wileyonlinelibrary.com]

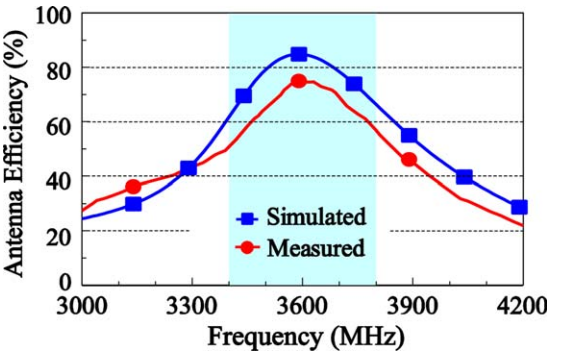

Figure 9 Measured and simulated antenna efficiencies of the fabricated DIFA. [Color figure can be viewed in the online issue, which is available at wileyonlinelibrary.com]

observed. The minimum S_{21} is shifted to lower frequencies with increasing inductance. The results indicate that the S_{21} can be controlled by the inductor L_d. In this study, the inductor is selected to be 39 nH, with which the maximum S_{21} over the 3.6-GHz band is the smallest (about −17.5 dB for 39 nH vs. −16 dB for 36 nH and −15 dB for 42 nH).

Effects of mounting the proposed DIFA at different positions along the top edge of the device ground plane are also analyzed. Figure 6 shows the simulated S parameters for the proposed DIFA at $d = 0$ (left corner position), 45 mm, and 90 mm (central position, see in Fig. 1). The S_{11} results show that for the $d = 0$ position, much better impedance matching for Ant1 in the proposed DIFA is obtained. This is probably because Ant1 is flushed to the left corner at $d = 0$, where the electric-field maximum of the device ground (chassis) resonant mode is usually located [11]. With the excitation of Ant1, an efficient coupling of the chassis resonant mode may occur, which improves the impedance matching and widens the impedance bandwidth as well. For Ant2, there are small variations in the S_{22} for the three different positions. It is largely because Ant2 is in the right-hand side of the DIFA, and hence, its coupling to the chassis resonant mode at the three positions is not significant. From the S_{21} results, relatively strong coupling is seen for the two IFAs in the DIFA at the $d = 0$ position. This behavior may also be related to the efficient coupling of Ant1 with the chassis resonant mode, which could lead to strong excitation of the surface currents on the device ground plane and in turn result in enhanced coupling of the two IFAs. For the proposed DIFA at $d = 90$ mm (the central position), the S_{21} is the smallest. This behavior may be because the electric-field minimum of the chassis resonant mode is usually located at its central position [11]. Hence, the coupling of the two IFAs with the chassis resonant mode is weak, and better isolation can be obtained.

3. EXPERIMENTAL RESULTS AND MIMO PERFORMANCE

3.1. Experimental Results

The proposed DIFA is fabricated, and Figure 7 shows the photos of the fabricated DIFA. The measured and simulated S parameters of the fabricated DIFA are presented in Figure 8. Agreement between the measurement and simulation is seen. The measured impedance matching with S_{11} better than −6 dB over the 3.6-GHz band is obtained, and the measured S_{21} is better than about −16.5 dB over the operating band.

Figure 9 shows the measured and simulated antenna efficiencies of the fabricated DIFA. The antenna efficiencies include the mismatching losses and were measured in a far-field

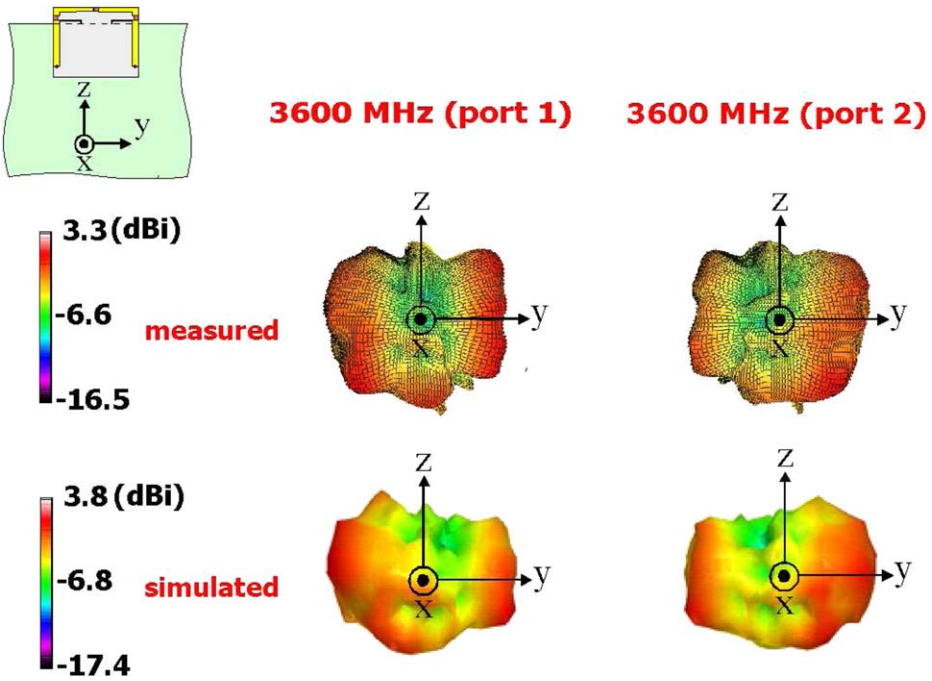

Figure 10 Measured and simulated 3D total-power radiation patterns of the fabricated DIFA. [Color figure can be viewed in the online issue, which is available at wileyonlinelibrary.com]

anechoic chamber. The measured antenna efficiency of about 50–74% is obtained over the operating band. The measured antenna efficiency is also seen to be about 10% lower than the simulated result. The discrepancies may be owing to the ohmic losses of the lumped chip inductors in the experiment. Figure 10 shows the measured and simulated three-dimensional (3D) total-power radiation patterns of the fabricated DIFA. The radiation patterns at 3600 MHz for port-1 and port-2 excitation are shown. Stronger radiation in the $-y$ direction than in the $+y$ direction is seen for the port-1 pattern. Conversely, stronger radiation in the $+y$ direction than in the $-y$ direction for the port-2 pattern is seen. The measured patterns also generally agree with the simulated patterns. This observation is reasonable, as the decoupling chip inductor L_d can block the excited surface currents from entering into Ant2 when port 1 is excited (see the results shown in Fig. 3), or vice versa. This behavior can make the port-1 and port-2 patterns with less similarity, which is advantageous for achieving smaller ECC and better channel capacity for MIMO operation.

3.2. MIMO Performance

Figure 11 shows the calculated ECC from the measured complex electric-field patterns and simulated ECC from the HFSS version 15 [10]. For the ECC results, the indoor propagation environment with uniform incident wave is assumed. That is, the cross-polarization power ratio (XPR) of the incident wave is set to 0 dB, and the θ and ϕ polarized power functions of the incident wave are both set to $1/4\pi$ in all directions. From the results, the calculated ECC is small, less than about 0.05, which is good for the MIMO operation [12]. The calculated ECC is also seen to agree with the simulated ECC.

Figure 12 shows the calculated channel capacities of the fabricated DIFA in a 2 × 2 MIMO system. In the capacity calculation, the uncorrelated transmitting antennas and the i.i.d. (independently identically distributed) channels with Rayleigh fading environment are assumed [13]. The capacities are obtained by averaging over 10,000 Rayleigh fading realizations with a signal-to-noise ratio of 20 dB at the fabricated DIFA.

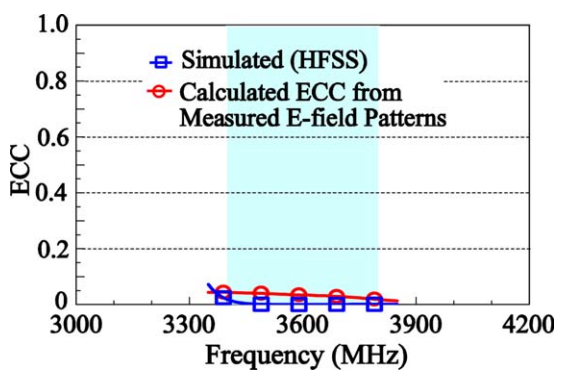

Figure 11 Calculated ECC from the measured complex electric-field patterns and simulated ECC from the HFSS. [Color figure can be viewed in the online issue, which is available at wileyonlinelibrary.com]

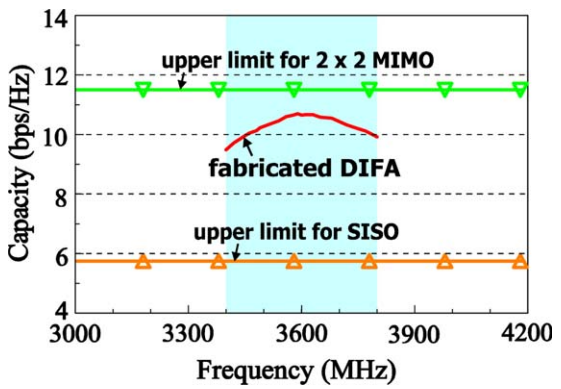

Figure 12 Calculated channel capacities of the fabricated DIFA in a 2 × 2 MIMO system. [Color figure can be viewed in the online issue, which is available at wileyonlinelibrary.com]

Over the operating band, the calculated capacities reach about 9.5–10.7 bps/Hz, which is significantly larger than the upper limit (5.75 bps/Hz) of a single-antenna (Single-Input Single-Output) with a perfect antenna efficiency of 100%. The calculated capacities are also close to the upper limit (11.5 bps/Hz) of a 2 × 2 MIMO system, in which the two antennas have perfect antenna efficiencies of 100% and a perfect ECC of 0. The results indicate that the proposed DIFA is promising for the LTE MIMO operation.

4. CONCLUSION

A DIFA with simple structure, small size, and acceptable isolation has been proposed for the 3.6-GHz LTE operation (3.4–3.8 GHz) in the tablet computer. The two IFAs therein are connected through a decoupling chip inductor at their open ends. It has been shown that acceptable isolation of the two IFAs can be obtained, which is largely because an equivalent bandstop circuit is formed owing to the decoupling chip inductor and the equivalent distributed capacitor between the open ends of the two IFAs. The measured isolation of the fabricated DIFA is better than 16.5 dB over the 3.6-GHz band, and the measured antenna efficiencies are better than 50%. The proposed DIFA also shows good MIMO performance, with the channel capacity in a 2 × 2 MIMO system reaching about 10.5–11.5 bps/Hz. The proposed DIFA is promising for the MIMO operation in the terminal communication device.

REFERENCES

1. X. Ling and R. Li, A novel dual-band MIMO antenna array with low mutual coupling for portable wireless devices, IEEE Antennas Wireless Propag Lett 10 (2011), 1039–1042.
2. S.W. Su, C.T. Lee, and F.S. Chang, Printed MIMO-antenna system using neutralization-line technique for wireless USB-dongle applications, IEEE Trans Antennas Propag 60 (2012), 456–463.
3. Y. Wang and Z. Du, A wideband printed dual-antenna system with a novel neutralization line for mobile terminals, IEEE Antennas Wireless Propag Lett 12 (2013), 1428–1431.
4. C.H. See, R.A. Abd-Alhameed, Z.Z. Abidin, N.J. McEwan, and P.S. Excell, Wideband printed MIMO/diversity monopole antenna for WiFi/WiMAX applications, IEEE Trans Antennas Propag 60 (2012), 2028–2035.
5. Y. Wang and Z. Du, A wideband printed dual-antenna with three neutralization lines for mobile terminals, IEEE Trans Antennas Propag 62 (2014), 1495–1500.
6. A. Cihangir, F. Ferrero, G. Jacquemod, P. Brachat, and C. Luxey, Neutralized coupling elements for MIMO operation in 4G mobile terminals, IEEE Antennas Propag Lett 13 (2014), 141–144.
7. K.L. Wong and T.W. Weng, Small-size triple-wideband LTE/WWAN tablet device antenna, IEEE Antennas Wireless Propag Lett 12 (2013), 1516–1519.
8. LTE frequency bands & spectrum allocations—A summary and tables of the LTE frequency band spectrum allocations for 3G & 4G LTE—TDD and FDD, Available at: http://www.radio-electronics.com/.
9. K.L. Wong and S.C. Chen, Printed single-strip monopole using a chip inductor for penta-band WWAN operation in the mobile phone, IEEE Trans Antennas Propag 58 (2010), 1011–1014.
10. ANSYS HFSS, Ansoft Corp., Pittsburgh, PA, Available at: http://www.ansys.com/products/.
11. J. Villanen, J. Ollikainen, O. Kivekas, and P. Vainikainen, Coupling element based mobile terminal antenna structures, IEEE Trans Antennas Propag 54 (2006), 2142–2153.
12. M.S. Sharawi, Printed multi-band MIMO antenna systems and their performance metrics, IEEE Antennas Propag Mag 55 (2013), 218–232.
13. A.A. Al-Hadi, J. Ilvonen, R. Valkonen, and V. Viikari, Eight-element antenna array for diversity and MIMO mobile terminal in LTE 3500 MHz band, Microwave Opt Technol Lett 56 (2014), 1323–1327.

A COMPACT ASYMMETRIC MONOPOLE ANTENNA WITH ELECTRICALLY COUPLED SRR FOR WIMAX/WLAN/UWB APPLICATIONS

V. Rajeshkumar and S. Raghavan
Department of Electronics and Communication Engineering, National Institute of Technology (NIT), Tiruchirappalli, Tamil Nadu, India; Corresponding author: vrajeshme@gmail.com

Received 5 March 2015

ABSTRACT: *In this article, a very compact printed asymmetric rectangular monopole antenna with an electrically coupled split ring resonator (SRR) is presented. The operating frequencies cover the worldwide interoperability for microwave access (WiMAX), wireless local area network (WLAN), and ultra wideband (UWB) applications. The asymmetric monopole is fed by a microstrip line, whereas the SRR is inductively coupled with the radiating element. The electric field-coupled SRR yields its resonance at 3.5 GHz in addition to the fundamental wideband resonance obtained by the asymmetric monopole. The measured operating bands (3.48–3.62 GHz), (5.1–11.12 GHz) are suitable for WiMAX and 5 GHz WLAN bands. Consequently, the overall operating bands of the antenna cover the UWB range with the exception of 3.1–3.48 and 3.62–5.1 GHz range. The proposed antenna has a very compact size of 13 × 15 × 1.6 mm^3.* © 2015 Wiley Periodicals, Inc. Microwave Opt Technol Lett 57:2194–2197, 2015; View this article online at wileyonlinelibrary.com. DOI 10.1002/mop.29298

Key words: *multiband; split ring resonator; worldwide interoperability for microwave access; wireless local area network; ultra wideband*

1. INTRODUCTION

Most commonly used wireless standards IEEE 802.16e worldwide interoperability for microwave access (WiMAX) and IEEE 802.11a wireless local area network (WLAN) demands for low cost, compact antennas. To meet these requirements, different multiband, wideband, and ultra wideband (UWB) antennas have been reported [1,2]. In general, multiband has been achieved by perturbing the surface current paths using fractal theory [3] as well as introducing various slots [4] in the radiating element. Further, asymmetrical feeding [5] has been used for reducing the antenna size. However, there is always a tradeoff between the size and multiband performance. Recent studies verified the miniaturization attained in antennas and waveguides using metamaterials [6–8]. The split ring resonator (SRR) is a kind of metamaterial cell, which has resonant nature due to the inductance and capacitance of the loop and split gap [1]. Hence, it has been efficiently used in various microwave/RF radiating and nonradiating printed circuits to enhance their performance. Metamaterial resonators (metaresonators) can be excited with a nearby feeding structure like transmission line or monopole by inductive/capacitive coupling. Hence, the SRR can radiate efficiently independent of the feeding structure's resonance [9]. Thus, it proves an effective way to reduce the antenna size.

In this letter, a compact asymmetrical monopole (half of the dimension compared with a rectangular patch) is used for achieving wideband performance. The asymmetrical monopole in turn is used to excite the SRR. Hence, the lowest resonance can be achieved by the metaresonator of very small size compared with its resonant wavelength, thereby reducing the overall size of the antenna.

2. PROPOSED ANTENNA CONFIGURATION

The proposed monopole antenna is printed on a 1.6 mm (h) FR-4 dielectric substrate with permittivity of 4.4 and loss tangent of